Quantitative Mapping of Free-Standing Lipid Membranes on Nano-Porous Mica Substrates

Luca Costa1, ‡; Adrian Carretero-Genevrier2, ‡,; Etienne Ferrain3,4; Pierre-Emmanuel Milhiet1,*; and Laura Picas5,*.*

AUTHOR ADDRESS

1Centre de Biochimie Structurale (CBS), CNRS UMR 5048 – Université de Montpellier, Montpellier, France.

2 Institut d'Électronique et des Systèmes (IES), CNRS UMR 5214 – Université de Montpellier, Montpellier, France.

3Institute of Condensed Matter and Nanosciences, Bio & Soft Matter (IMCN/BSMA), Université Catholique de Louvain, Louvain-la-Neuve, Belgium.

4it4ip s.a., Louvain-la-Neuve, Belgium.

5Institut de Recherche en Infectiologie de Montpellier (IRIM) and CNRS UMR 9004, Montpellier, France.

‡These authors contributed equally.

*Corresponding author.

KEYWORDS

Atomic Force Microscopy (AFM), nano-mechanics, quantitative imaging, biological membranes.

ABSTRACT

The physic-chemistry of biological membranes is at the origin of fundamental cellular functions such as vesicle trafficking, cell adhesion and migration[1-3]. Because most of intracellular shapes and local demixing of membranes take place in the nanometer scale, AFM becomes an extremely powerful technique to assess the properties of these biological membranes. Porous substrates provide an elegant strategy to avoid the conundrum of placing soft and thin biomembranes on hard substrates for AFM studies, although the surface chemistry make the actual substrates rather challenging setups. Here, we have engineered porous systems on the most widely used substrate in AFM, mica muscovite, with tunable pore sizes from some tens to few hundreds nanometers for biological applications. We show that free-standing bilayers on nano-porous can be obtained by using well-established vesicle spreading methods and that they display equivalent nano-mechanical stability and phsyco-chemical properties to that of membranes on conventional mica supports. By reducing the pore radius < 40 nm and limiting the contribution of membrane tension to the elastic response of free-standing membranes we estimate a bending modulus of 18 k_bT and 73 k_bT for DOPC and DPPC bilayers, respectively. The quantitative mapping of suspended membranes shows a different mechanical response at the pore rims, which is more pronounced for DPPC and suggest a different lipid ordering. We find that the combination of membrane bending and the different lipid packing at the edges of pores shapes the curvature of free-standing membranes on pores in the range of few tens of nm.

INTRODUCTION

Biological membranes are essential components of cells by providing a physical boundary to the extracellular environment and the intracellular compartmentalization of organelles. Cellular membranes are 5 nm-thick heterogeneous composites made of a wide diversity of proteins and lipids with different structural and functional properties. The interplay between the biochemical and mechanical properties of membranes is at the origin of fundamental processes such as exo- and endocytosis, cell adhesion and migration[1-3]. To infer on the mechanical response of cellular membranes, bottom-up synthetic approaches provide a straightforward strategy by controlling several parameters such as the lipid composition, membrane organization or protein-lipid interactions[4]. Atomic Force Microscopy (AFM) has been widely used to asses the nanoscale properties of these synthetic minimal systems[5], as a result of its unique capabilities to probe the sample's mechanics while accessing to its topographical features, which becomes a major advantage for those lipid mixtures displaying phase separation at the nm- to meso-scale[5]. However, this comes at the expenses of placing thin and soft samples, such as biological membranes, on solid supports. Indeed, the contribution of the underlying substrate on the mechanical response of biological membranes as well as on other physico-chemical parameters such as lipid mobility in the membrane plane[6] or the lipid symmetry/asymmetry[7] should not be neglected. Several analytical methods have been proposed to overcome the contribution of a hard substrate on the AFM mechanical measurements of soft samples[8-9], although these approaches do not take into consideration the physico-chemical contributions. An interesting alternative to tackle the contribution of the underlying substrate is the engineering of free-standing biological membranes on porous substrates[10-12]. This strategy has been successfully applied on porous silicon[12], alumina[13], silicon nitride[14], or gold-coated silicon nitride[15] substrates. However, the main drawback of the current porous substrates used on AFM studies is linked to their surface chemistry, which makes difficult to obtain a large and homogeneous formation of supported lipid

bilayers by classic methods, as well as the eventual spontaneous rupture of membranes on large pores (hundreds of nm to micrometers)[16].

Here, we have taken advantage of the most widely used substrate in AFM, which is muscovite mica, to engineer nano-porous mica substrates of tunable pore sizes from some tens to few hundreds nanometers for biological applications. We have validated the suitability of nano-porous mica substrates by assessing the physico-chemical properties of DOPC:DPPC (1:1, mol/mol) lipid bilayers at the nanoscale using AFM. As a result, we provide a straightforward strategy to produce free-standing biomembranes that open up multiple applications in the AFM field. By performing nano-indentaiton experiments and quantitative mapping of free-standing membranes suspended on pores of different radius we have evaluated the elastic response and the correlation between the mid-plane curvature of suspended membranes and pore radius, both for DOPC and DPPC lipid phases. Our results provide an original strategy to probe the mechanical properties of biological membranes, including the bending modulus, with access to the lateral organization and heterogeneity of membranes in the range of tens of nm, which could be further extended to other relevant lipid mixtures and biological systems.

RESULTS

Control of pore size and crystallinity of porous mica substrates by chemical etching

Mica substrates are among the most widely used supports for high-resolution AFM observations of biological samples, as they provide a hydrophilic and atomically flat surface. Moreover, they offer the possibility of exfoliation, a feature that largely improves sample quality by exposing clean mica surfaces upon each delamination. To produce porous mica substrates with improved porous tracks depth, we chose high energy and heavy Xe ions to irradiate mica wafers over other lighter ions or particles[17]. In addition, this type of ion tracks should provide the possibility to further develop the substrates by soft chemical etching. As a result, mica wafers

where irradiated with 420 MeV Xe ions accelerated using a cyclotron (Cyclotron Research Center, Louvain-la-Neuve, Belgium and GANIL, Caen, France). We produced a random distribution of rhombic shape nano-pores with a controlled pore dimension, as shown by the AFM topographic characterization of nano-porous mica substrates (Figure 1). The pore size was controlled by the etching time of Xe irradiated mica substrates (see methods) and remained stable after 3-4 exfoliation cycles, as confirmed by AFM and electron microscopy (Figure 2). Pore size distribution as a function of the different etching times was established by AFM from the projected area of the pores and then fitted by assuming a circular shape of radius *R* (nm). The average pore radius obtained at each of the etching conditions tested was designed to be 12.9 ± 1.0 nm, 20.4 ± 3.0 nm, 32.6 ± 2.1nm, 42.1 ± 4.5 nm and 82.3 ± 0.87 nm, as shown in Figure 1C. The pore density was optimized at $1 \cdot 10^{9}$ cm^{-2} (Figure 1A). High-resolution AFM imaging at the pores rims confirmed that the Xe ion irradiation and further chemical etching did not render the outmost mica layers amorphous as shown by Fast-Fourier Transform (FFT) analysis (Figure 1B). In addition, we could observe several mica terraces at the edges of mica pores (see cross-section analysis in Figure 1B).

The size and crystallinity of nano-porous mica tracks is stable over tens of microns

To further confirm the crystallinity of the nano-porous mica substrates and establish the pore length we performed a structural characterization of the samples by Field-Emission Scanning Electron Microscopy (FE-SEM) and Transmission Electron Microscopy (TEM) (Figure 2). FE-SEM analysis of nano-porous mica substrates confirmed a remarkable porous length over several tens of microns (see Figure 2A and 2B). Moreover, we also observed that the pore size established by the etching time was constant all along the ion tracks (Figure 2C and magnified region, Figure 2D). TEM images and Electron diffraction analysis confirmed that nano-porous mica substrates display an atomically flat single crystalline surface with a uniform diameter of the track-etched pores (see Figure 4D and Figure 4E). Electron diffraction pattern along the [001] zone axis showed the high crystallinity and crystallographic planes corresponding to the

facets of the rhombic porous (see yellow dashed dots in Figure 2E). The indexed and reconstructed unit cell of nano-porous mica substrates confirmed that our substrates present a monoclinic cell with lattice parameters a=5.19 Å, b=9,04Å, c=20.08Å β=95.5°. Importantly, this unit cell has the symmetry expended for the 2M1 muscovite structure[18].

Free-standing lipid bilayers on nano-porous mica substrates are mechanically stable

Next, we evaluated the suitability of the nano-porous mica substrates to obtain continuous lipid bilayers suitable for AFM studies (Figure 3). To this end, we chose a lipid mixture consisting of DOPC:DPPC (1:1, mol/mol) because is amongst the best characterized lipid mixtures in AFM studies and thus, a suitable *in vitro* model to correlate our observations with previous works[19]. Also, this lipid mixture makes possible to evaluate the behavior of liquid (L_α, for the DOPC) and gel (L_β, for the DPPC) lipid phases at room temperature. DOPC:DPPC lipid bilayers on nano-porous mica substrates where obtained by classic methods[20] (see methods section). AFM analysis of these samples showed the presence of liquid and gel phase separation, in agreement with previous studies using classic mica substrates[19]. In addition, we confirmed that the resulting lipid bilayers are continuous and without the absence of apparent defects over several tens of micrometers (Figure 3A). This feature was also confirmed by epifluorescence microscopy of DOPC bilayers doped with 0.1% of DOPE-rhodamine. Altogether, suggesting that that formation of lipid bilayers on nano-porous mica substrates by classic methods, such as the spreading of small unilamellar vesicles, has a yield comparable to that of classic mica supports.

We then evaluated the stability of free-standing lipid bilayers on nano-porous mica substrates by performing a topographical mapping of DOPC and DPPC phases spanning over pores of R = 42.1 ± 4.5 nm (Figure 3C). The AFM characterization of liquid and gel phases at minimal loading forces (i.e. 100 pN) confirmed the existence of free-standing bilayers for the two phases and showed a profile analysis that is more pronounced in the absence than in the presence lipid

bilayers and for the DOPC over the DPPC lipids, respectively. The absence of membrane rupture at any of the setpoint loading forces tested also confirmed that free-standing lipid bilayers on nano-porous mica substrates are mechanically stable, at least, up to 500 pN, both for the fluid and gel lipid phases (Figure 3C).

To validate that the chemical etching and the subsequent exfoliation of the outmost mica layers provide DOPC:DPPC (1:1, mol/mol) lipid membranes comparable to that of conventional mica substrates we evaluated the elastic properties of both lipid phases away from nano-pores, i.e. on supported lipid bilayer (SLBs) (Figure S2). We estimated the Young's modulus (*E*) of both DOPC and DPPC supported lipid bilayers by fitting the Hertz model to retracting force-distance (FvD) curves acquired upon static force spectroscopy measurements. The resulting *E* was of 13.3 MPa and 19.1 MPa for the fluid and gel phase, respectively, and was in quantitative agreement with previous studies performed on SLBs of the same lipid composition[19]. Taken together, these observations point out that free-standing bilayers on nano-porous mica substrates display equivalent nano-mechanical stability and properties to that of conventional mica supports.

The mechanical response of free-standing bilayers is modulated by the pore size

The mechanical response of free-standing lipid bilayers on porous substrates is mainly governed by the membrane tension and bending modulus at moderate AFM indentations, since membrane stretching is rather prevented by the flow of membrane towards the pore rims. Thus, for lipid membranes suspended on large pore's radius, *R*, of several hundreds of nm, the elastic response is primarily dictated by the lateral tension of the membrane, as previously suggested[14]. This is not the case for smaller pore's sizes, where the membrane bending could eventually dominate over tension and thus, become the main mechanical contribution to AFM indentations[16]. This behavior is well supported by theoretical predictions and experimental findings on large pores[14], but there is current lack of mechanical studies on smaller pore's sizes that could provide a complete picture of the mechanical response of free-standing membranes. Therefore, we

monitored the mechanical response of free-standing membranes of DOPC and DPPC in the elastic regime as a function of the pore radius, R (R = 20.4 ± 3.0 nm, 32.6 ± 2.1nm, 42.1 ± 4.5 nm and 82.3 ± 0.87 nm) (Figure 4). For each of the aforementioned pore radius we performed static force spectroscopy measurements at moderate indentation forces of 100 – 150 pN and FvD curves were recorded (typical indentation curves obtained are displayed in Figure S1). The apparent stiffness (K_{eff}) of DOPC and DPPC lipid membranes was estimated by linear fitting of FvD curves performed at the center of each of the four different pore radius tested (Figure 4A-B). The resulting K_{eff} on DOPC bilayers was 38.0 ± 5.8 nN·μm^{-1}, 22.0 ± 6.3 nN·μm^{-1}, 13.0 ± 2.8 nN·μm^{-1}, and 13.9 ± 7.5 nN·μm^{-1}, respectively. In the case of DPPC lipid phases we obtained a K_{eff} of 153.7 ± 38.5 nN·μm^{-1}, 70.3 ± 8.5 nN·μm^{-1}, 14.0 ± 2.8 nN·μm^{-1}, and 17.6 ± 2.3 nN·μm^{-1}, respectively. To confirm that long-range interaction forces would not provide an overestimation of our quantifications we evaluated the deformation of lipid bilayers at two loading forces: 100 pN and 150 pN (Figure S3). As expected, our measurements showed larger deformation values at 150 pN for both DOPC and DPPC lipid bilayers and for any of the pore sizes tested. In addition, we found that membrane deformation increases with the pore size and reaches a plateau at pore sizes of $R \geq$ 42.1 ± 4.5 nm for both DOPC and DPPC phases.

By invoking thin plate theory, the membrane bending, κ, can be estimated by assuming a point load force F acting on a clamped free-standing membrane suspended on a pore with radius R[14,21]:

$$F = \frac{4\pi E h^3}{3(1-\nu^2)R^2}\delta = \frac{64\pi\kappa}{R^2}\delta \quad (1)$$

where h is the bilayer thickness[22], ν the Poisson ratio, and δ indentation depth. We found that the K_{eff}·R^2 increases with pore radius and would reach a plateau at radius $R >$ 42.1 ± 4.5 nm therefore, suggesting that above this pore sizes other components than bending modulus might

contribute to the mechanical response of free-standing membranes. Indeed, this observation is agreement with previous findings suggesting that increasing pore radius would limit the possibility to evaluate the membrane bending as a result of the curvature stress exerted by the AFM tip[14]. Consequently, from our experimental data on free-standing membranes of DOPC and DPPC on the porous substrates of $R = 20.4 \pm 3.0$ nm we estimated a bending modulus of 18 k_bT and 73 k_bT, respectively. Importantly, these values are in quantitative agreement with previous estimations of the same lipid mixture[19, 22-23].

Finally, we assessed the potential heterogeneity in the mechanical properties of free-standing lipid bilayers we performed high-resolution quantitative mechanical mapping of DOPC and DPPC phases suspended on pores of different radius ($R \approx 20$ to 40 nm) (Figure 4C-D for DOPC and DPPC, respectively). As expected, we found a well differentiated apparent stiffness between supported and suspended DOPC and DPPC lipid bilayers, which supports the results displayed in Figure 4 A-B from single-point force spectroscopy measurements acquired at the center of pores. Interestingly, we found slight changes in the apparent stiffness at the pore rims of both DOPC and DPPC, which could suggest different lipid packing. Indeed, this intermediate stiffness, which ranged from few to tens of nm, was particularly remarkable in the case of DPPC, possibly as a result of the increased lipid ordering and the shear-stress forces of gel phases.

Collectively, our experimental data suggest that the mechanical response of free-standing bilayers is likely modulated by the pore radius with two well-defined trends around $R \approx 40$ nm, with a contribution of membrane bending below this pore size and dominated by the membrane tension at larger pore's radius (Figure 4E).

The pore size shapes the curvature of free-standing lipid membranes

A fundamental feature of cellular membranes is related to their ability to be shaped, a process that is typically assisted by dedicated proteins that can either introduce lipid bilayer asymmetry

or apply a mechanical constrains to force membranes to bend[24-25]. The energy needed to bend a membrane and thus, undergo a given curvature is, in general terms, related its bending modulus and to the membrane tension[26]. Since we found that the pore rim might display different lipid ordering and that membrane bending is likely to contribute to the elastic response of free-standing membranes at pore radius $R \leq$ 40 nm (Figure 4), we asked whether the pore size could influence the shape of free-standing membranes. To this end, we performed high-resolution contact point mapping of DOPC and DPPC lipid membranes suspended on pores with radius $R \leq$ 40 nm (Figure 5 and Figure S4). Briefly, the contact point mapping is based on the acquisition of series of FvD curves at each pixel of the image and the subsequent rendering of a topography image, where the height is determined by the force at which the tip gets into contact with the sample, i.e. the contact point. As the contact point mapping minimizes the peak forces exerted on the sample it should reveal its unperturbed topography profile. Using this approach we have evaluated the relationship between the mid-plane membrane curvature as a function of the pore radius for both DOPC and DPPC free-standing membranes, as shown in Figure 5A and B. Interestingly, in both cases we found a correlation between the pore size and the curvature of suspended membranes, which was more pronounced in the case of free-standing DOPC lipid membranes. Indeed, we observed that for the same pore sizes DOPC lipid membranes shape into more curved membranes, possibly as a result of their lower membrane rigidity and thus, bending energy, compared to gel phases. Taken together, these results suggest that sub-hundred nanometer pores are able to shape the curvature of liquid and gel lipid bilayers and that this feature is possibly dictated by the interplay between membrane bending and eventual changes in lipid ordering at pore rims.

DISCUSSION

The engineering of porous substrates provides an effective strategy to circumvent the conundrum of the underlying substrate on AFM measurements[11-12, 14, 27], which might become a

critical issue in the case of thin and soft samples such as biological membranes. However, the material's chemistry of the actual porous substrates make them quite challenging systems to engineer biological membranes, in addition to the difficulty to transpose well-established methods already developed on classic mica substrates. In the present work we have engineered nano-porous mica substrates of tunable pore sizes from some tens to hundred nanometers for biological applications. Our structural and surface characterization of these substrates (Figure 1 and 2) points out that by using high energy and heavy Xe ions to irradiate mica wafers and soft chemical etching we can obtain well-defined pore sizes (Figure 1C) with a constant radius throughout the porous track (Figure 2A-B). This finding importantly supports the potential of using this method on thinner mica sheets (< 10 µm) to engineer two separating aqueous compartments with wide number of biological applications (e.g. on ion pumps, voltage gated channels, etc). We have validated the suitability of nano-porous mica substrates by evaluating a widely established lipid mixture in the AFM field such as DOPC:DPPC (1:1, mol/mol). Our results show that by using classic vesicle spreading methods, which is among the most used methods to obtain biomembranes in AFM studies, we can produce lipid bilayers that are continuous over tens of micrometers (Figure 3A-B) and that display equivalent mechanical properties to that obtained on classic mica substrates (Figure S2). Therefore, confirming that well-established methods in AFM can be transposed and thus, no additional optimization steps need to be considered when using nano-porous mica substrates. The obtention of large and homogenous membranes might be an additional advantage (Figure 3B), as no further fluorescence microscopy is required to pinpoint the regions of the sample containing membrane patches[16]. In addition, our results show that free-standing membranes of DOPC and DPPC on nano-porous mica substrates are mechanically stable up to 500 pN (Figure 3C), a feature that prevents the chances of eventual spontaneous membrane rupture that is often observed on substrates with larger pore sizes[16]. Altogether, supporting the suitability of nano-porous mica substrates to assess the physico-chemical properties of biological membranes at the nanoscale without the drawbacks of an underlying hard substrate.

The physic-chemistry of biological membranes plays a major role in a wide number of fundamental cellular functions: from vesicle trafficking to cytoskeleton-mediated processes[1-3], as stated above. A common feature of all these processes is linked to the ability of membranes to be bent and thus, to undergo shape changes that are generally assisted by specialized molecular machines[28]. Importantly, in the case of vesicle trafficking membranes typically display strongly curved shapes in the nanometer range ($R \approx 20$ to 50 nm)[29]. Not to mention the growing number of studies pointing out that local demixing of lipid molecules in the membrane plane, possibly in the nm range, might be relevant to orchestrate trafficking and signaling process[30]. However, the number of techniques allowing for the correlation of physical properties, such as membrane curvature, with the chemical organization of cellular membranes at the nanoscale is rather limited[4, 31]. In this work we have made a step forward by assessing the elastic properties of biological membranes at a nanometer relevant scale in biology by engineering nano-porous mica substrates with pore radius from 20 to 80 nm to suspended lipid bilayers displaying the coexistence of liquid (L_α, for the DOPC) and gel (L_β, for the DPPC) lipid phases. Importantly, we found that the mechanical behavior of free-standing bilayers is not homogenous with an intermediate apparent stiffness between supported-suspended lipid membranes at the boundary of the pore's rim (Figure 4C and 4D). The fact that this feature was more pronounced in the case of free-standing lipid bilayers consisting of a gel phase (Figure 4D, $R \approx 40$ nm) strengthens the hypothesis that differences in lipid packing might be at the origin of this heterogeneity. Since membrane curvature can arise from lipid bilayer asymmetry with respect to the membrane plane[29], we assessed whether the eventual different lipid ordering at the supported-suspended lipid membrane interface of DOPC and DPPC bilayers might eventually assist changes in membrane shape. By performing high-resolution contact-point mapping (Figure S4) in of free-standing membranes suspended at different pore radius ($R \approx 20$ to 40 nm) we found a correlation between the mid-plane curvature of suspended membranes and pore radius for both fluid and gel phases (Figure 5D and E). This behavior was more pronounced in the case of DOPC lipid

bilayers, i.e. for an equivalent pore radius DOPC free-standing membranes are display smaller mid-plane curvature than DPPC membranes. Thus, suggesting that in addition to the eventual different lipid packing at the pore's rim, other parameters such as the intrinsic deformability of membranes might also plays a role in the shaping free-standing membranes on nano-pores. Indeed, we found that DOPC lipid bilayers display a lower bending modulus (18 k_bT) than DPPC membranes (73 k_bT), as assessed from the experimental data shown in Figure 4 and in quantitative agreement with the values reported in the litarature[19, 22-23]. It is well reported that parameters such as membrane bending and tension as well as lipid composition and packing are relevant to determine the degree of membrane curvature[28, 32]. In the case of porous systems, the contribution to the elastic response of free-standing membranes at moderate indentations is dominated by the lateral tension and bending modulus for pore size from $R \approx$ 60 nm down to tens of nm, as previously anticipated[16]. Indeed, by finely tuning the size of nano-porous mica substrates we could confirm the existence of two well-defined trends in the mechanical behavior of pore-spanning membranes, as shown by the relationship between $K_{eff} \cdot R^2$ of DOPC and DPPC suspended bilayers as a function of pore radius (Figure 4A and B). In our porous system, we found that $K_{eff} \cdot R^2$ reaches a plateau at above pore radius 40 $\geq$ nm. Interestingly, in the case of DOPC we estimated a K_{eff} of $\approx$ 14 nN·μm^{-1} for pore $R \geq$ 40 nm, which is in agreement with the apparent stiffness previously obtained on phosphatidylcholine pore-spanning membranes on larger pores radius $R \geq$ 600 nm[15]. Altogether, supporting the fact that at larger pore sizes other components than membrane bending might contribute to the elastic response of free-standing lipid bilayers for both DOPC and DPPC membranes (equation 1). This observation could explain the fact that close to $R \approx$ 35 the mid-plane curvature of free-standing membranes is approaches to zero (i.e. flat membrane) for both DOPC and DPPC (Figure 5A-C), possibly as a result of the contribution of membrane tension to the elastic response of suspended membranes at

larger pore radius. Therefore, the combination of membrane bending and the different lipid packing at the edges of pores might be relevant to shape the curvature of free-standing membranes suspended on small pore radius, i.e. $R \leq 40$ nm. Therefore, resulting into singular membrane curvatures for both liquid and gel phases (Figure 5B-C): whereas DOPC membranes would display a large bending modulus and possibly, lower lipid packing at the pore rims, DPPC membranes exhibit a lower bending modulus but a remarkable difference in lipid ordering at the boundary of pores. It is tempting to speculate that on a more complex cellular context the existence of a configuration that would mimic a suspended bilayer might contribute in generating or initiating membrane curvature, although to a lower extend to that of specialized molecular motors[29]. Interestingly, the expected mesh size of cortical cytoskeleton networks (i.e. 30-150 nm)[33] correlates well with the window of pore radius that we found to be relevant to shape suspended membranes, thus suggesting a potential correlation between membrane curvature and pore/mesh size in a biologic relevant context.

CONCLUSIONS

In conclusion, we have presented experimental data supporting the suitability of a new method to engineer free-standing biomembranes, with equivalent physic-chemical properties to that of widely used mica wafers therefore, opening up large number of future applications of nano-porous mica in the AFM field: from chemistry to physics and biology. By controlling the pore size radius we have shown the potential of our method to probe the elastic properties of biological membranes, including the bending modulus, with improved access to the lateral organization and heterogeneity of membranes in a biological relevant range of tens of nm. Finally, we have investigated the mechanisms of curvature creation on nano-porous systems by applying high-resolution quantitative imaging, including contact-point mapping, to map the mechano-chemistry of free-standing membranes at the nanoscale.

METHODS

Nano-Porous Mica Substrates

Nano-porous mica substrates were obtained following a similar experimental approach as in[17]. In the present work, mica substrates were exposed to 420 MeV MeV energy Xe ions. Exposure to high-energy ions produced depth local defects on mica sheets (Muscovite Mica V-1 Quality, 71855-01, Electron Microscopy Sciences) and consequently remarkable porous length over several tens of microns. Irradiated mica wafers were then immersed in 20 wt.% HF (11.4 M) at different etching times. Because the etching rate was several orders of magnitude higher around damaged regions in comparison with unexposed mica regions, increasing etching time results in enlargement of the pores size around the local defects. The relation between the etching time (min) *versus* the pore radius (nm) obtained is displayed in Figure 1C. The pore radius, *R*, was estimated from AFM images of uncleaved nano-porous mica substrates and estimated as detailed in the AFM data analysis section.

Lipid Bilayer Preparation

1,2-dipalmitoyl-sn-glycero-3-phosphocholine (DPPC), 1,2-dioleoyl-sn-glycero-3-phosphocoline (DOPC) were purchased from Avanti Polar Lipids, Inc. DOPC:DPPC (1:1, mol/mol) Lipid Bilayers (LBs) were prepared following the protocol previously reported[19]. Briefly, DPPC and DOPC were dissolved in chloroform:methanol (2:1, vol/vol) in a glass tube. Then, the solvent was evaporated under nitrogen flow in order to obtain a thin film. The lipid film was then hydrated with a buffer solution of 10mM Tris (pH 7.4), 150 mM NaCl prepared with ultrapure water (Milli-Q reverse osmosis system, 18.2 mΩ cm resistivity) to a final concentration of 0.2 mM. The obtained suspension was extruded through a polycarbonate membrane filter (100 nm pores size, Whatman) to obtain small unilamellar vesicles. (SUVs). 50 μL of SUVs solution were deposited onto freshly nano-porous mica (1 cm diameter, 100 μm thick). LBs were formed

during 30 min incubation at 70ºC, followed by incubation at room temperature for 10 min, then rinsed 10 times with the buffer solution.

AFM Experiments

AFM experiments were performed on a Nanowizard 3 AFM (JPK), except for the characterization of nano-porous mica substrates that were performed on a Multimode IV AFM (Bruker). All experiments were performed in fluid (10mM, Tris (pH 7.4), 150 mM NaCl). Unless stated otherwise V-shaped Silicon nitride tips with a nominal tip radius of 2 nm[19] on 0.1 N/m or 0.6 N/m cantilevers were used (MSNL, Bruker). Cantilever spring constant and sensitivity were calibrated on a contact-based operation using thermal tuning (JPK Nanowizard or Nanoscope 8 software). Characterization of porous mica substrates was performed in Peak-Force Quantitative Nano-Mechanical Mapping (PF-QNM, Bruker) mode at a setpoint loading force of 200 pN. Atomically resolved AFM images of nano-porous mica were obtained in Amplitude-Modulation mode (AM-AFM) with AC55 cantilevers (Olympus) with nominal spring constant and tip radius 85 N/m and 7 nm, respectively. Nano-indentation experiments were performed by first acquiring an image of a single pore and then, acquiring FvD curves in static mode AFM Force Spectroscopy at the center of the pore by indenting with forces of 0.2 nN-0.5 nN at a rate of 3-5 $\mu m \cdot s^{-1}$. Quantitative mapping of free-standing membranes was performed at a scan size of 300 nm x 300 nm and 600 nm x 600 nm (256 lines x 256 pixels). Force setpoint was set at 100 to 200 pN for DOPC and 200 to 500 pN for DPPC free-standing membranes. To achieve a high quality approach-retract FvD curve at each pixel of the sample, the amplitude of the tip was set at 40 - 70 nm and the tip speed at 10 $\mu m \cdot s^{-1}$. These parameters were optimized to maximize the S/N ratio for each FvD curve, leading to an accurate evaluation of the contact point at each pixel of the image.

Electron Microscopy

Porous mica structure was assessed using a field emission gun scanning electron microscope (FEG-SEM), Hitachi's SU77. Transmission electron microscopy (TEM) studies were performed using a FEI Titan3 operated at 300kV and equipped with a superTwin® objective lens and a CETCOR Cs-objective corrector from CEOS Company. Specimens for TEM observation were prepared by standard dispersion of the sample with ultrasonic device during 10 min and then deposited on carbon coated grid. Electron diffraction experiments were performed using a Jeol 1210 transmission electron microscope operating at 120 KV, equipped with a side-entry 60/30º double tilt GATHAN 646 analytical specimen holder.

AFM data analysis

AFM data analysis was performed using the JPKSPM data processing software and Gwyddion[34], a modular open-source software for SMP data analysis (gwyddion.net). The average radius of nano-porous mica substrates was obtained by applying a mask with an automated threshold method on AFM images that were previously flattened. Statistical pores size distribution was obtained by evaluating the projected surface area of individual pores (N ≥ 100 pores per condition). Adjacent pores were not considered in the data treatment. Finally, the obtained area was fitted into the area of a circle of a given radius, R. The apparent stiffness (K_{eff}) of either supported or suspended bilayers was obtained from the slope in the contact region of FvD curves of either static force spectroscopy measurements or on individual curves obtained at each pixel of the image in the case of the quantitative mapping. The deformation was designed as the tip penetration at the setpoint force and was estimated from FvD curves acquired by performing static force spectroscopy measurements. The measured Young's modulus (E) on supported lipid bilayers was estimated from the contact region of the retracting FvD curve using by fitting the Hertz model of a parabolic tip of radius R = 5 nm indenting an elastic half-space[19,35],

$$F = \frac{4\sqrt{R}}{3}\frac{E}{1-\nu^2}\delta^{3/2}$$

where δ is the indentation and ν the Poisson ratio ($\nu = 0.5$). The contact point mapping was generated through post-processing of each of the FvD curves obtained at each pixel of the image using the JPKSPM data processing software by placing the image setpoint at the force at which the tip contacts the sample's surface therefore, creating a final topography image at the contact point, i.e. in the absence of peak forces.

FIGURES

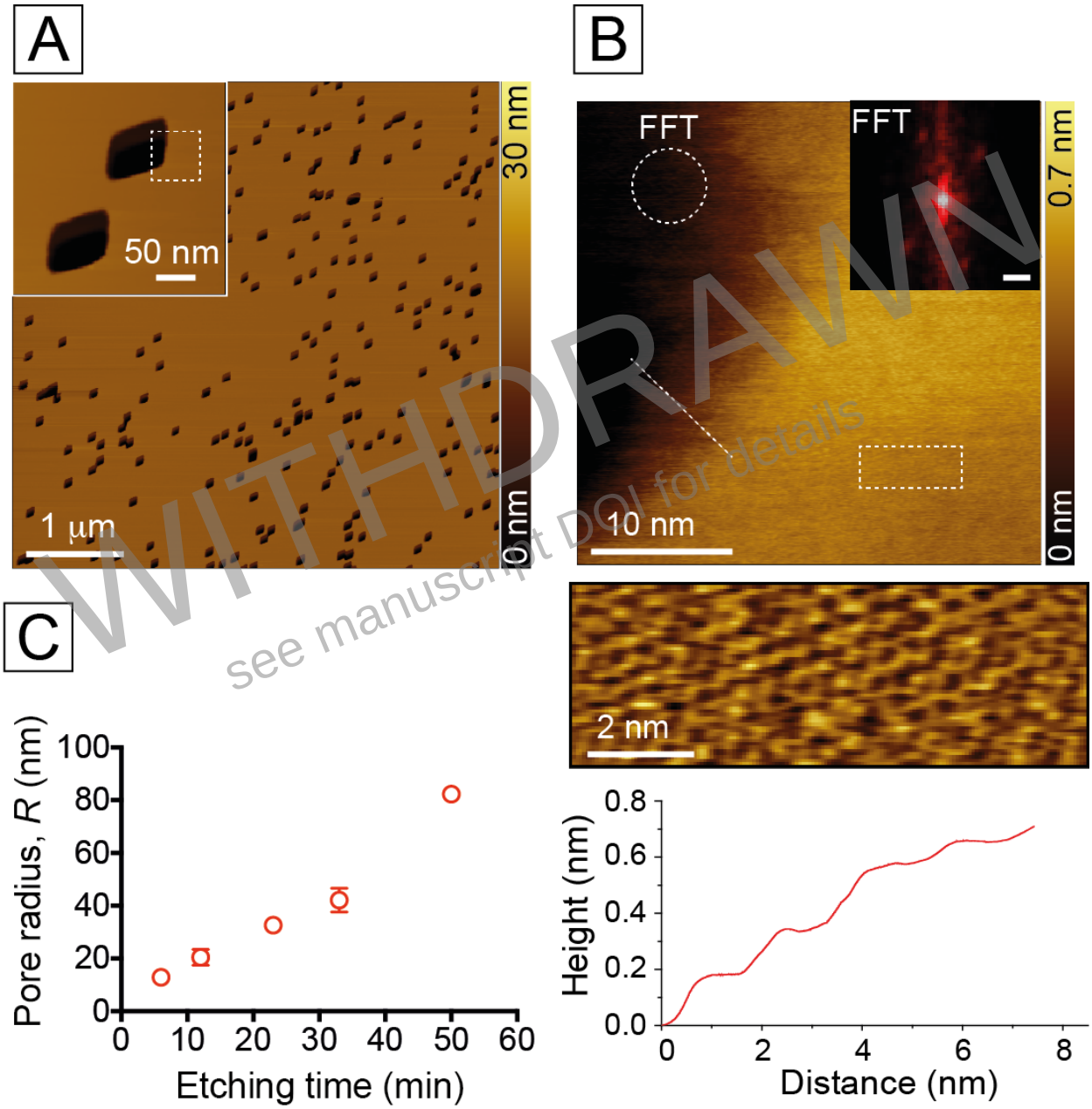

Figure 1. Surface characterization of nano-porous mica substrates by AFM. **(a)** Large scan AFM topography image of nano-porous mica substrates etched for t ≈ 25 min and cleaved before imaging. Inset shows a detail of the obtained porous morphology afer chemical etching. (b) AFM image acquired at the pore's rim (upper panel, highlighted in inset of a) showing the crystallinity

of nano-porous mica substrates after etching assessed by Fast-Fourier transform on the dashed circle (FFT on inset) and by high-resolution imaging on the dashed rectangle (middle panel). Profile analysis along the dashed line in b showing the mica terraces that compose the pore's rim after etching (lower panel). (c) Quantification of the relationship between etching time (min) and the obtained pore radius (*R*, nm) on nano-porous mica substrates obtained as detailed in the methods section.

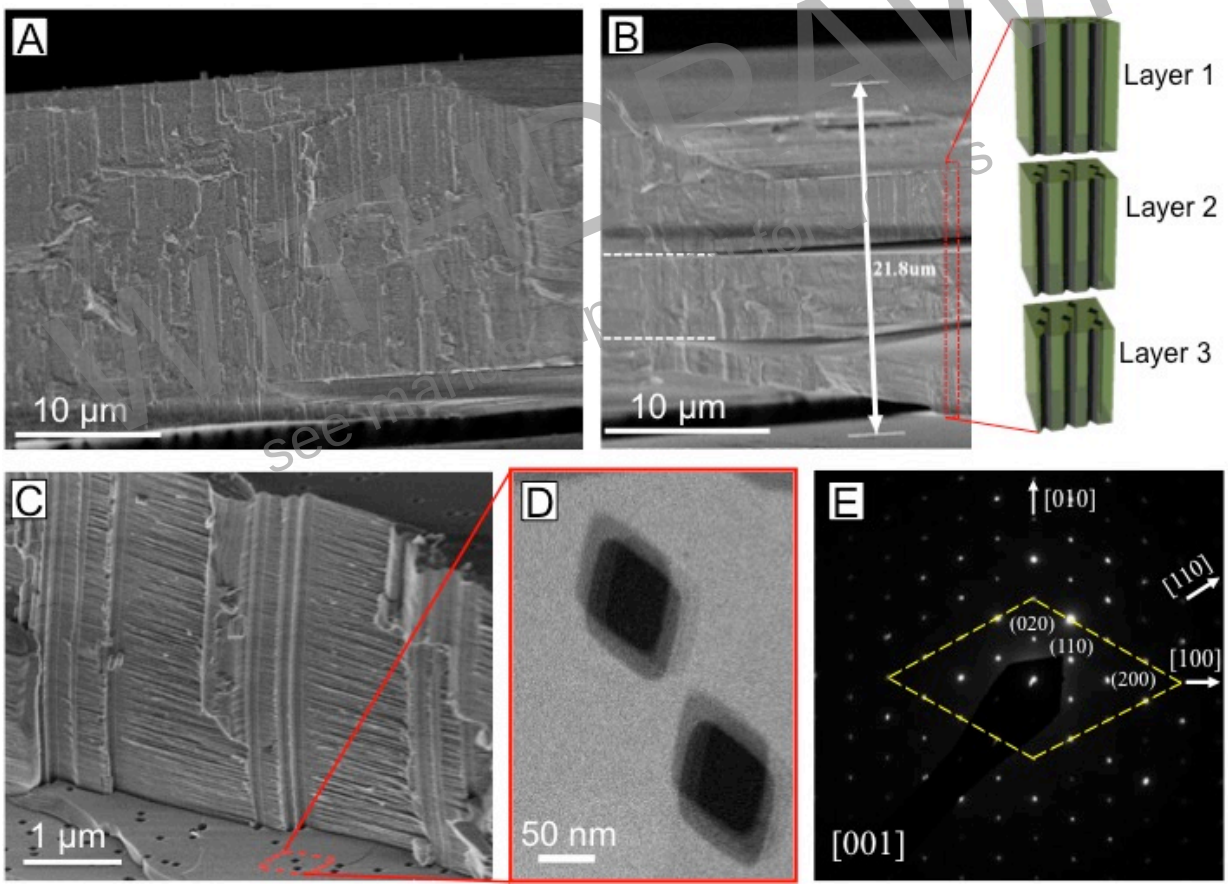

Figure 2. Structural characterization of nano-porous mica substrates by Electron Microscopy. (**a**) Cross-sectional view SEM-FEG image of porous mica showing the regular distribution, diameter and alignment of nanochannels over several microns of thickness. (**b**) Cross-sectional view SEM-FEG image of porous mica substrate showing the possibility to produce 3-4 porous exfoliation cycles of a same wafer. (**c**) Detailed SEM-FEG image of regular porous channels in track-etched mica substrate. (**d**) Low resolution HAADF TEM image of two pores with long axis

dimension of 90 nm. (e) Electron diffraction pattern of image d along the [001] zone axis that shows the high crystallinity and crystallographic planes corresponding to the facets of rhombic shape porous. The indexed unit cell of porous mica substrate corresponds to a monoclinic cell with lattice parameters a=5.19Å, b=9,04Å, c=20.08Å β=95.5°. This reconstructed unit cell corresponds to a 2M1 muscovite structure.

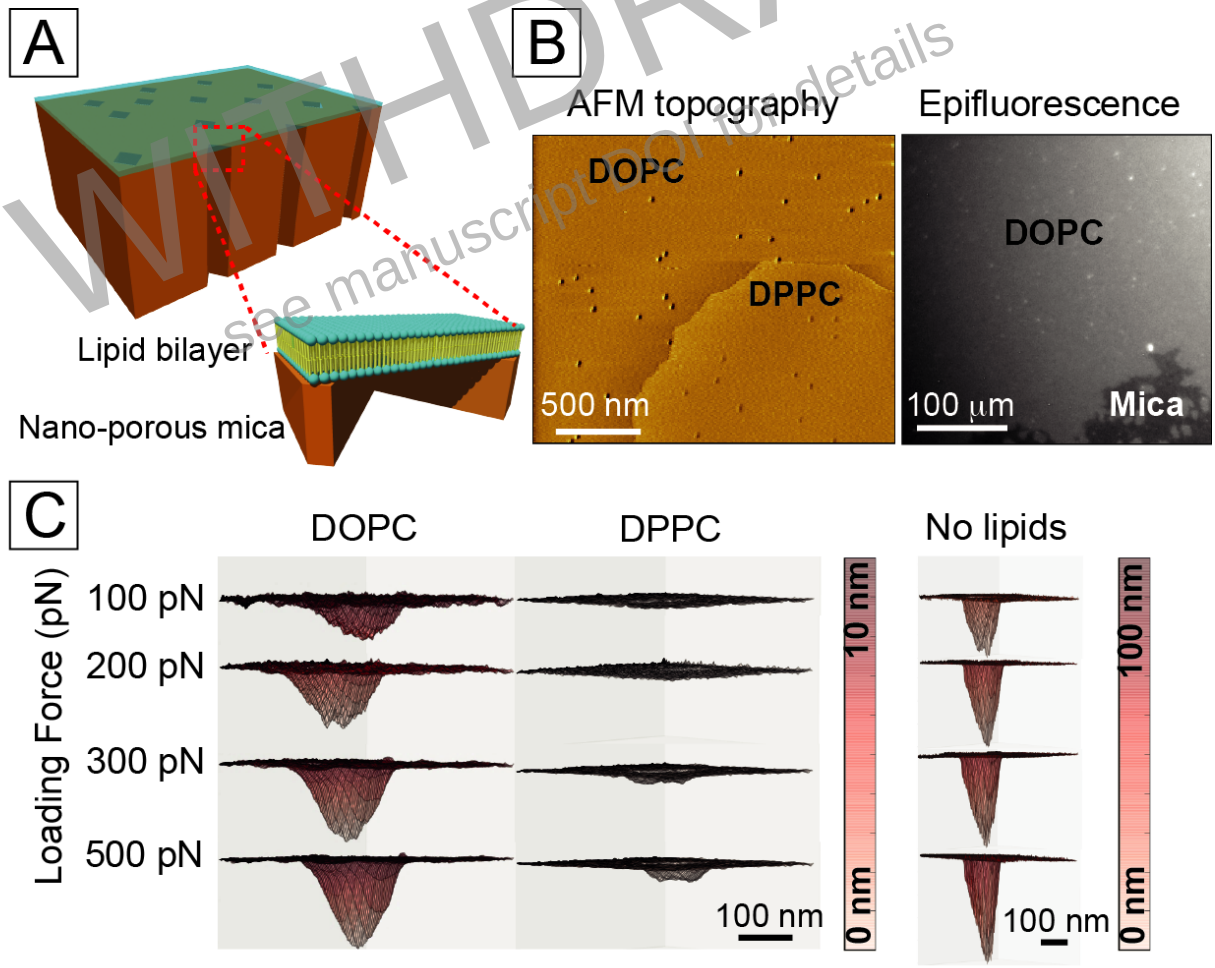

Figure 3. Stability of free-standing lipid membranes on nano-porous mica substrates. (a) Schematic representation of supported and suspended lipid bilayers on nano-porous mica

substrates. (b) Typical AFM topography image of DOPC:DPPC (1:1, mol/mol) lipid bilayers obtained on nano-porous mica substrates displaying separation between liquid (L_α, for the DOPC) and gel (L_β, for the DPPC) lipid phases at room temperature (left). Epifluorescence image of DOPC bilayers doped with 0.1% of DOPE-rhodamine obtained on nano-porous mica substrates. (c) 3D profile analysis of suspended membranes of DOPC and DPPC on nano-porous mica substrates of $R \approx 40$ nm acquired at different setpoint loading forces (100 pN, 200 pN, 300 pN, and 500 pN) (left). Control experiment was performed on the same porous substrates in the absence of lipid bilayers showing that in the absence of suspended membranes there is a $\geq$ 10-fold increase in the profile depth (no lipids, right).

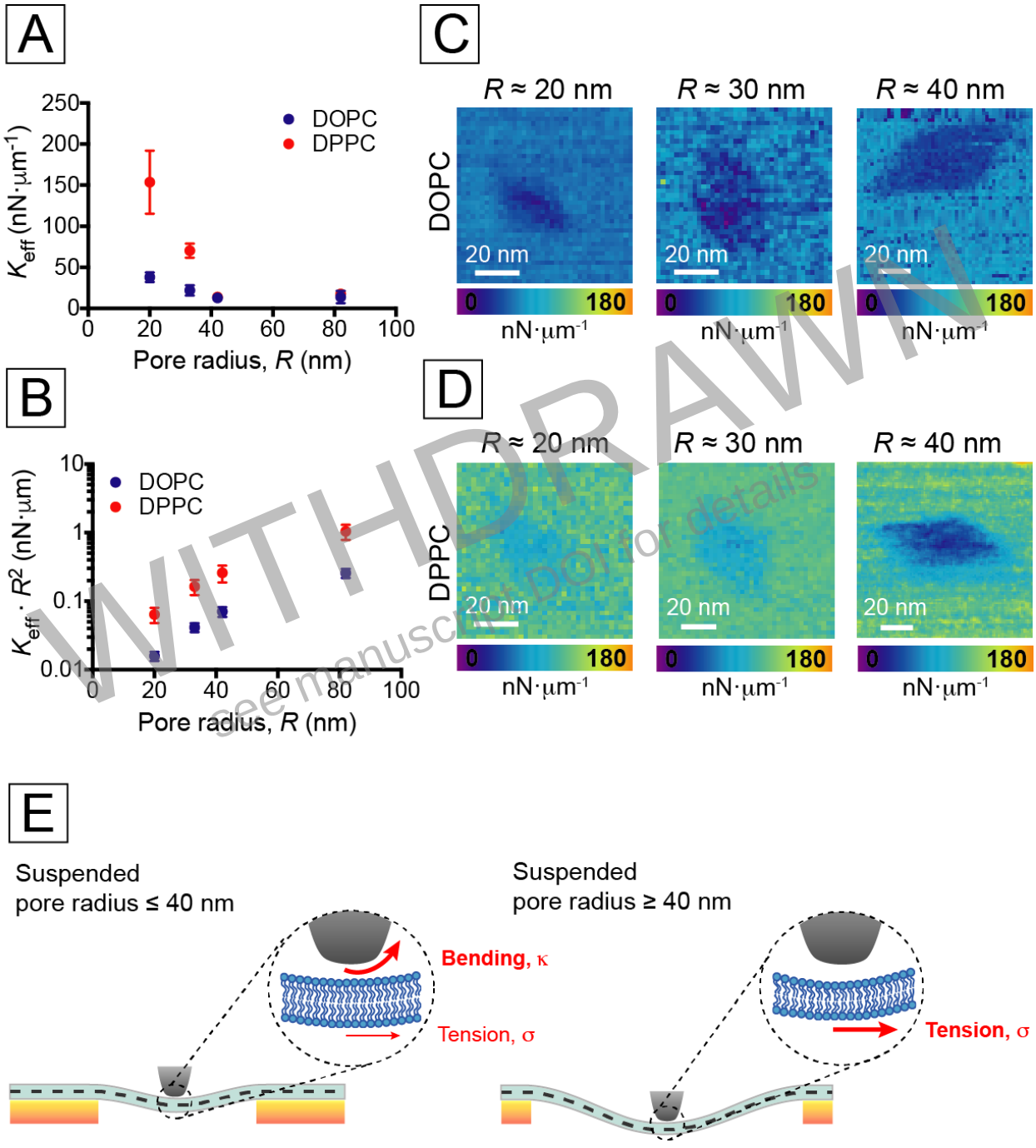

Figure 4. Quantitative nano-mechanics of free-standing lipid membranes on nano-porous mica substrates. (a) Representation of the apparent stiffness (K_{eff}) of DOPC (blue dots) and DPPC (red squares) lipid bilayers suspended on different pore radius (R ≈ 20.4 nm, 32.6 nm, 42.1 nm, and 82.3 nm) obtained from FvD curves acquired at the center of different pores (st.d., N ≥ 5)

for each of the conditions tested. (b) Representation of $K_{eff} \cdot R^2$ of free-standing DOPC (blue dots) and DPPC (red squares) lipid as a function of the pore radius R ≈ 20.4 nm, 32.6 nm, 42.1 nm, and 82.3 nm. (c, d) Representative quantitative nanomechanical maps showing the different distribution of the apparent stiffness (K_{eff}) of DOPC (c) and DPPC (d) suspended lipid bilayers on pores of R ≈ 20 nm, 30 nm, 40 nm. (e) Schematic representation of the mechanical response of free-standing bilayers at low indentation forces. Based on the experimental data obtained in a and b two conditions are displayed: pore $R \geq$ 40 nm showing that the mechanical response is dominated by the tension in the membrane plane (σ) and $R \leq$ 40 nm, where both membrane bending ($\varkappa$) and tension contribute to the mechanics of free-standing membranes under an AFM tip.

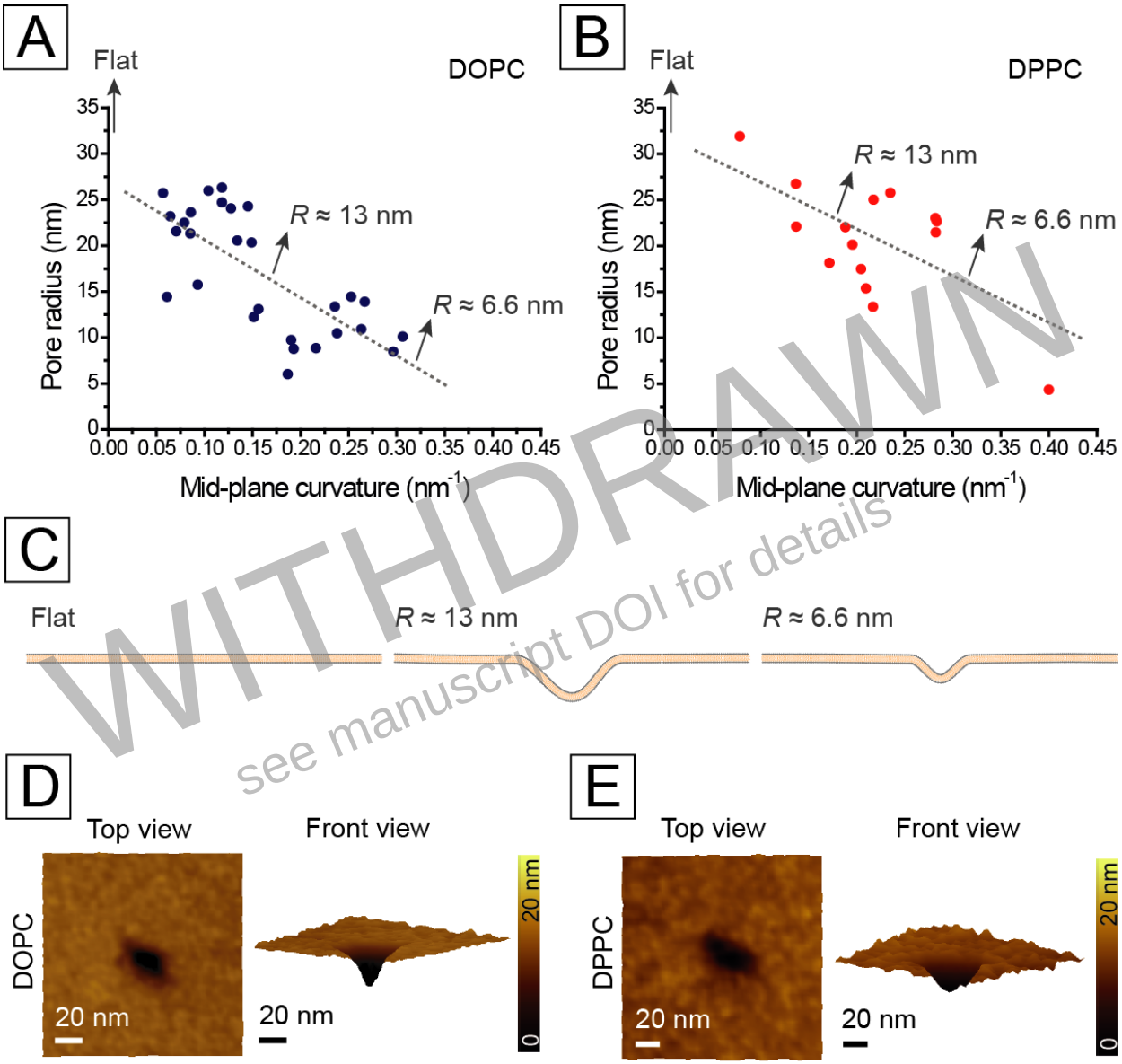

Figure 5. Pore size and curvature of free-standing lipid membranes. (a, b) Representation of the mid-plane curvature of DOPC (blue dots, a) and DPPC (red dots, b) suspended lipid membranes as a function of the pore radius (*R*). Curvature values where estimated from contact-point maps to reveal the shape of membranes with negligible effect of peak forces on the image's topographic features. (c) Schematic picture of the representative membrane shapes obtained from the experimental data shown in images a and b: flat membrane and membrane with a mid-plane curvature of R ≈ 13 nm and 6.6 nm. (d, e) Top and front view of representative of contact-point

maps showing the shape of DOPC (d) and DPPC (e) suspended lipid membranes on pores of R ≈ 20 nm.

ASSOCIATED CONTENT

Supporting Information.

Supporting Information includes details on the nano-mechanical characterization of supported and free-standing lipid bilayers on nano-porous mica substrates (Figure S1-S3) as well as on the contact-point mapping of samples (Figure S4).

AUTHOR INFORMATION

Corresponding Author

* E-mail: laura.picas@irim.cnrs.fr

* E-mail: carretero@ies.univ-montp2.fr

* E-mail: pem@cbs.fr

ORCID

Laura Picas: 0000-0002-5619-5228

Author Contributions

A.C-G and L.P designed the project. L.C, A.C-G, E.F and L.P performed experiments. L.C, A.C-G and L.P analyzed data. A.C-G and P-E.M provided equipment and reagents. A.C-G and L.P wrote the manuscript.

Funding Sources

LP acknowledges the financial support of the program ATIP-Avenir. ACG acknowledges the financial support from the French Agence Nationale pour la Recherche (ANR), projet Q-NOSS

ANR ANR-16-CE09-0006-01 and the Ecole Centrale de Lyon under the BQR 2016 project. The research leading to these results also received funding from the European Union Seventh Framework Programme under Grant Agreement 312483 - ESTEEM2 (Integrated Infrastructure Initiative–I3) to ACG and support of the Labex EpiGenMed to LC.

ACKNOWLEDGMENT

The authors would like to thank Dr. David Montero to assist with the electron microscopy and Dr. José M. Villa-Fungairiño for assistance in chemical etching. Dr. Félix Rico and Dr. Manouk Abkarian for fruitful discussions. FEGSEM instrumentation was facilitated by the Institut des Matériaux de Paris Centre (IMPC FR2482) and was funded by UPMC, CNRS and by the C'Nano projects of the Région Ile-de-France.

ABBREVIATIONS

AFM, Atomic Force Microscopy; FE-SEM, Field-Emission Scanning Electron Microscopy; TEM, Transmission Electron Microscopy ; FFT, Fast-Fourier Transform; DOPC, 1,2-dioleoyl-sn-glycero-3-phosphocoline; DPPC, 1,2-dipalmitoyl-sn-glycero-3-phosphocholine; FvD, force versus distance curve.

REFERENCES

1. Diz-Munoz, A.; Fletcher, D. A.; Weiner, O. D., Use the force: membrane tension as an organizer of cell shape and motility. *Trends Cell Biol* **2013**, *23* (2), 47-53.
2. Gauthier, N. C.; Masters, T. A.; Sheetz, M. P., Mechanical feedback between membrane tension and dynamics. *Trends Cell Biol* **2012**, *22* (10), 527-35.
3. Sheetz, M. P., Cell control by membrane-cytoskeleton adhesion. *Nat Rev Mol Cell Biol* **2001**, *2* (5), 392-6.
4. Lagny, T. J.; Bassereau, P., Bioinspired membrane-based systems for a physical approach of cell organization and dynamics: usefulness and limitations. *Interface Focus* **2015**, *5* (4), 20150038.
5. Picas, L.; Milhiet, P. E.; Hernandez-Borrell, J., Atomic force microscopy: a versatile tool to probe the physical and chemical properties of supported membranes at the nanoscale. *Chem Phys Lipids* **2012**, *165* (8), 845-60.
6. Dertinger, T.; von der Hocht, I.; Benda, A.; Hof, M.; Enderlein, J., Surface sticking and lateral diffusion of lipids in supported bilayers. *Langmuir* **2006**, *22* (22), 9339-44.

7. Richter, R. P.; Mukhopadhyay, A.; Brisson, A., Pathways of lipid vesicle deposition on solid surfaces: a combined QCM-D and AFM study. *Biophys J* **2003**, *85* (5), 3035-3047.
8. Gavara, N.; Chadwick, R. S., Determination of the elastic moduli of thin samples and adherent cells using conical atomic force microscpe tips. *Nature Nanotechnology* **2012**.
9. Dimitriadis, E. K.; Horkay, F.; Maresca, J.; Kachar, B.; Chadwick, R. S., Determination of elastic moduli of thin layers of soft material using the atomic force microscope. *Biophys J* **2002**, *82* (5), 2798-810.
10. Sonnleitner, A.; Schutz, G. J.; Schmidt, T., Free Brownian motion of individual lipid molecules in biomembranes. *Biophys J* **1999**, *77* (5), 2638-42.
11. Steltenkamp, S.; Müller, M. M.; Desemo, M.; Hennesthal, C.; Steinem, C.; Janshoff, A., Mechanical properties of pore-spanning lipid bilayers probed by atomic force microscopy. *Biophys. J.* **2006**, *91*, 217-226.
12. Goncalves, R. P.; Agnus, G.; Sens, P.; Houssin, C.; Bartenlian, B.; Scheuring, S., Two-chamber AFM: probing membrane proteins separating two aqueous compartments. *Nat Methods* **2006**, *3* (12), 1007-12.
13. Nussio, M. R.; Oncins, G.; Ridelis, I.; Szili, E.; Shapter, J. G.; Sanz, F.; Voelcker, N. H., Nanomechanical characterization of phospholipid bilayer islands on flat and porous substrates: a force spectroscopy study. *J Phys Chem B* **2009**, *113* (30), 10339-47.
14. Mey, I.; Stephan, M.; Schmitt, E. K.; Muller, M. M.; Ben Amar, M.; Steinem, C.; Janshoff, A., Local membrane mechanics of pore-spanning bilayers. *J Am Chem Soc* **2009**, *131* (20), 7031-9.
15. Kocun, M.; Lazzara, T. D.; Steinem, C.; Janshoff, A., Preparation of solvent-free, pore-spanning lipid bilayers: modeling the low tension of plasma membranes. *Langmuir* **2011**, *27* (12), 7672-80.
16. Janshoff, A.; Steinem, C., Mechanics of lipid bilayers: What do we learn from pore-spanning membranes? *Biochim Biophys Acta* **2015**, *1853* (11 Pt B), 2977-83.
17. Sun, L.; Chien, C. L.; Searson, P. C., Fabrication of nanoporous single crystal mica templates for electrochemical deposition of nanowire arrays. *Journal of Materials Science* **2000**, *35* (5), 1097-1103.
18. Güven, N., *The crystal structure of 2M1 phengite and 2M1 muscovite*. Carnegie Inst. Washington Year Book: 1967; Vol. 66.
19. Picas, L.; Rico, F.; Scheuring, S., Direct Measurement of the Mechanical Properties of Lipid Phases in Supported Bilayers. *Biophys J* **2012**, *102* (1), L01-L03.
20. Richter, R. P.; Berat, R.; Brisson, A., Formation of solid-supported lipid bilayers: an integrated view. *Langmuir* **2006**, *22* (8), 3497-505.
21. Komaragiri, U.; Begley, M. R., The mechanical response of freestanding circular elastic films under point and pressure loads. *J Appl Mech-T Asme* **2005**, *72* (2), 203-212.
22. Rawicz, W.; Olbrich, K. C.; McIntosh, T.; Needham, D.; Evans, E., Effect of chain length and unsaturation on elasticity of lipid bilayers. *Biophys J* **2000**, *79* (1), 328-39.
23. Dieluweit, S.; Csiszar, A.; Rubner, W.; Fleischhauer, J.; Houben, S.; Merkel, R., Mechanical properties of bare and protein-coated giant unilamellar phospholipid vesicles. A comparative study of micropipet aspiration and atomic force microscopy. *Langmuir 26* (13), 11041-9.
24. Jarsch, I. K.; Daste, F.; Gallop, J. L., Membrane curvature in cell biology: An integration of molecular mechanisms. *J Cell Biol* **2016**, *214* (4), 375-87.
25. Zimmerberg, J.; Kozlov, M. M., How proteins produce cellular membrane curvature. *Nature Reviews Molecular Cell Biology* **2006**, *7* (1), 9-19.
26. Helfrich, W., Elastic Properties of Lipid Bilayers - Theory and Possible Experiments. *Zeitschrift Fur Naturforschung C-a Journal of Biosciences* **1973**, *C 28* (11-1), 693-703.
27. Heinemann, F.; Schwille, P., Preparation of Micrometer-Sized Free-Standing Membranes. *Chemphyschem* **2011**, *12* (14), 2568-2571.
28. Kozlov, M. M.; Campelo, F.; Liska, N.; Chernomordik, L. V.; Marrink, S. J.; McMahon, H. T., Mechanisms shaping cell membranes. *Curr Opin Cell Biol* **2014**, *29*, 53-60.

29. Graham, T. R.; Kozlov, M. M., Interplay of proteins and lipids in generating membrane curvature. *Curr Opin Cell Biol* **2010,** *22* (4), 430-6.
30. Picas, L.; Gaits-Iacovoni, F.; Goud, B., The emerging role of phosphoinositide clustering in intracellular trafficking and signal transduction. *F1000Research* **2016,** *5*.
31. Gleisner, M.; Mey, I.; Barbot, M.; Dreker, C.; Meinecke, M.; Steinem, C., Driving a planar model system into the 3rd dimension: generation and control of curved pore-spanning membrane arrays. *Soft Matter* **2014,** *10* (33), 6228-6236.
32. Pinot, M.; Goud, B.; Manneville, J. B., Physical aspects of COPI vesicle formation. *Mol Membr Biol 27* (8), 428-42.
33. Morone, N.; Fujiwara, T.; Murase, K.; Kasai, R. S.; Ike, H.; Yuasa, S.; Usukura, J.; Kusumi, A., Three-dimensional reconstruction of the membrane skeleton at the plasma membrane interface by electron tomography. *J Cell Biol* **2006,** *174* (6), 851-62.
34. Nečas, D.; Klapetek, P., Gwyddion: an open-source software for SPM data analysis. *Central European Journal of Physics* **2012,** *10* (1), 181-188.
35. Hertz, H., Hertz's Miscellaneous Papers. Macmillan: London, 1881; pp 146–162.

Supporting information

Quantitative Mapping of Free-Standing Lipid Membranes on Nano-Porous Mica Substrates

Luca Costa1, ‡; Adrian Carretero-Genevrier2, ‡,; Etienne Ferrain3,4; Pierre-Emmanuel Milhiet1,*; and Laura Picas5,*.*

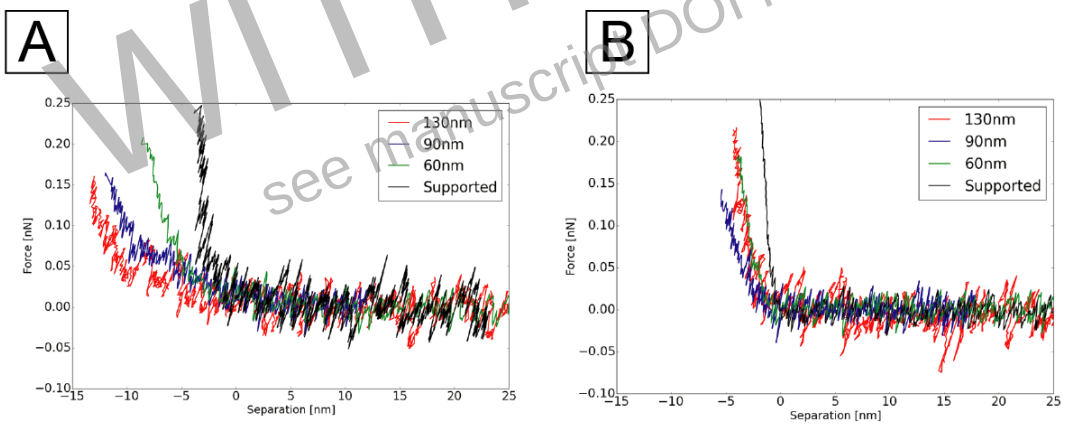

Figure S1. Representative FvD curves acquired on supported lipid bilayers (supported) and on free-standing lipid bilayers of DOPC (a) or DPPC (b) suspended on pores of different diameters. In this case, FvD were acquired at the center of the pore.

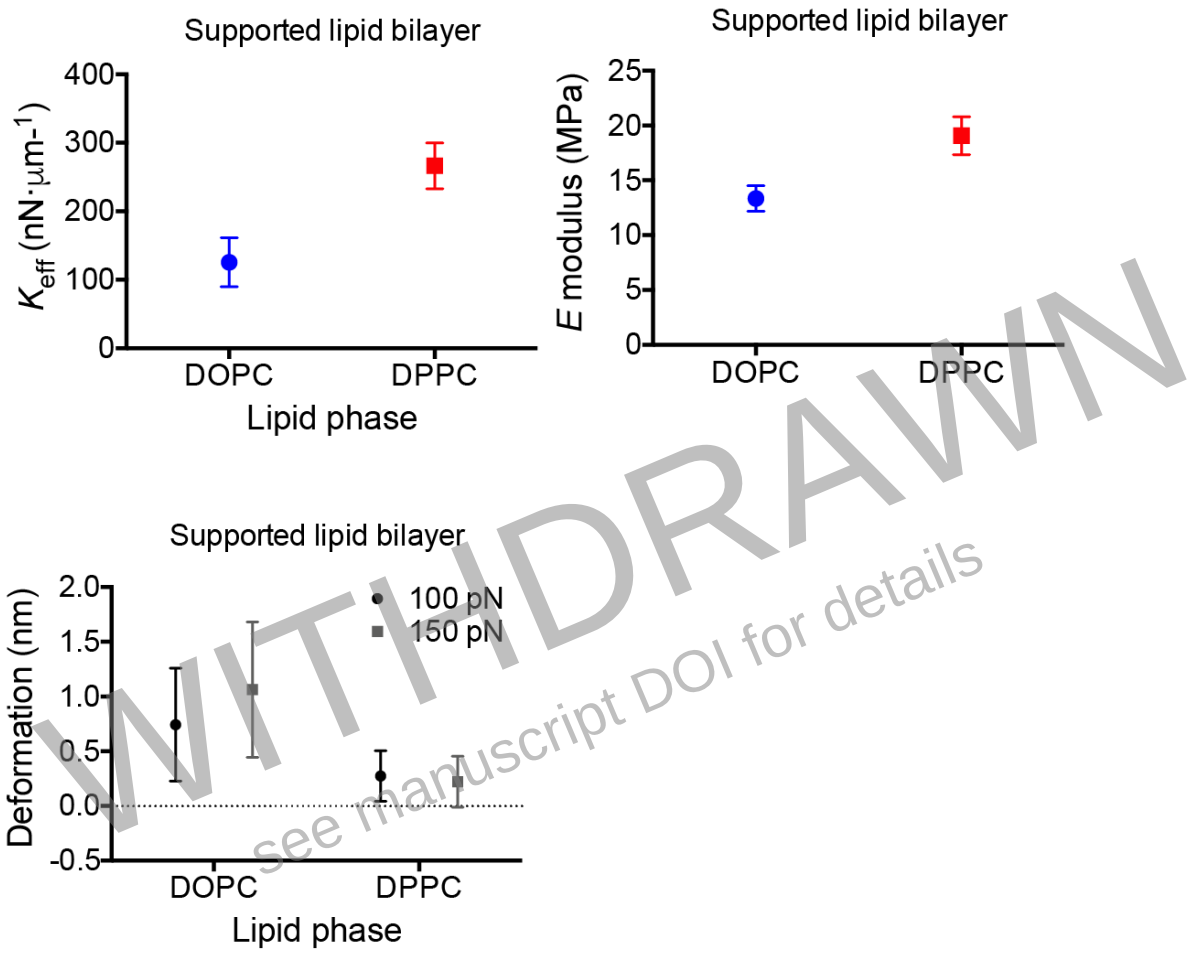

Figure S2. Representation of the apparent stiffness (K_{eff}) of DOPC (blue dots) and DPPC (red squares) supported lipid bilayers (st.d., N ≥ 5) (left, upper panel). Representation of the Young's modulus of DOPC (blue dots) and DPPC (red squares) supported lipid bilayers (st.d., N ≥ 5) (right, upper panel). Representation of the deformation of DOPC and DPPC supported lipid bilayers at a loading force of 100 pN (black dot) and 150 pN (gray square) (left, bottom panel) (st.d., N ≥ 5).

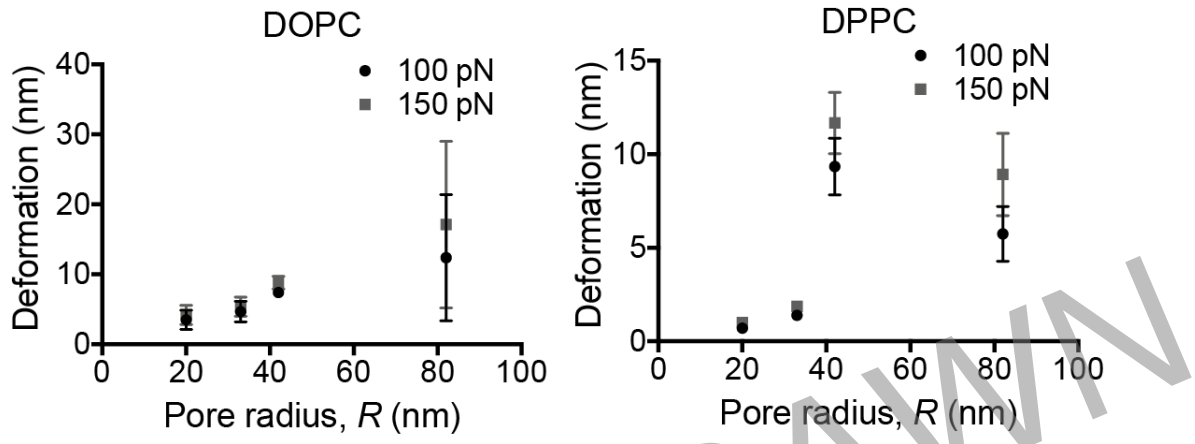

Figure S3. Representation of the deformation of DOPC (left panel) and DPPC (right panel) free-standing lipid bilayers at a loading force of 100 pN (black dot) and 150 pN (gray square) (left, bottom panel) (st.d., N ≥ 5).

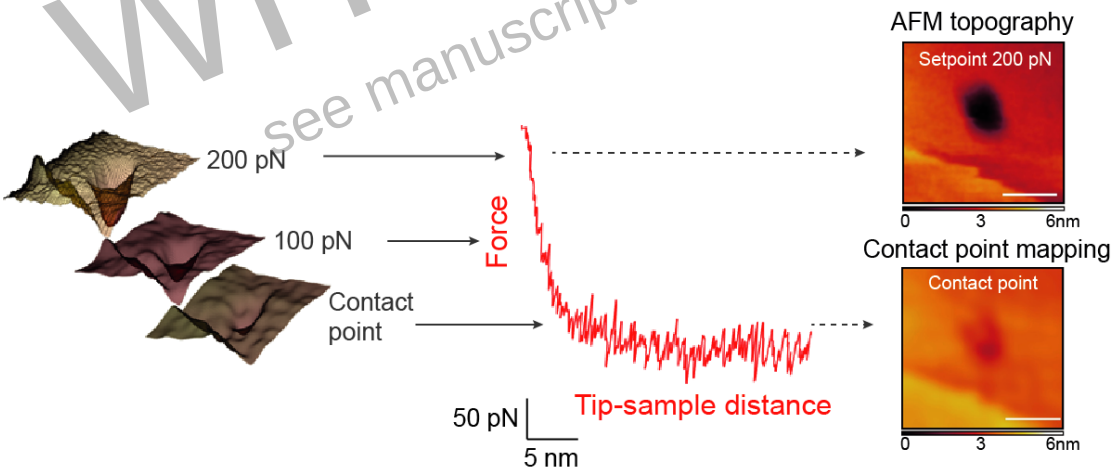

Figure S4. Schematic representation of the contact-point mapping showing the topographic features of a suspended lipid bilayer showing a coexistence of DOPC (dark region) and DPPC phases (light region) acquired at a setpoint force of 200 pN and at the minimal force, i.e the contact point.